Molecular ion irradiations of molybdenum

Mike Jenkins, Colin A English

Molecular ion irradiations of molybdenum

Journal:	*Philosophical Magazine & Philosophical Magazine Letters*
Manuscript ID:	TPHM-09-Feb-0071.R1
Journal Selection:	Philosophical Magazine
Date Submitted by the Author:	15-Jul-2009
Complete List of Authors:	Jenkins, Mike; University of Oxford, Materials English, Colin; National Nuclear Laboratory, Harwell Business Centre; University of Oxford, Department of Materials
Keywords:	defect analysis, radiation damage
Keywords (user supplied):	displacement cascades, cascade collapse

Molecular ion irradiations of molybdenum

C A English[a,b] and M L Jenkins[b,1]

[a] National Nuclear Laboratory, Harwell Business Centre, Didcot, Oxon OX11 0QJ

[b] Department of Materials, University of Oxford, Parks Road, Oxford OX1 3PH

[1] Corresponding author: Email: mike.jenkins@materials.ox.ac.uk

Abstract

A series of TEM experiments has been carried out to investigate systematically the formation of vacancy dislocation loops in displacement cascades in molybdenum. Single-crystal foils of high-purity molybdenum were irradiated with Sb^+ single ions and Sb_2^+ and Sb_3^+ molecular ions to low doses ($\leq 10^{16}$ ions m^{-2}). Three different ion energies were employed (60, 120 and 180 keV) in order to vary systematically the total cascade energy and the energy per atom in the molecular ion. Dislocation loop sizes and defect yields were found to be larger for molecular ions than for single ions of the same energy. In (011) foils most loops had Burgers vectors **b** = a/2<111> lying in the plane of the foil. However in molecular ion irradiations a small fraction of loops with **b** = a<100> was also found. This fraction was higher for Sb_3^+ than for Sb_2^+ ions and also increased with ion energy. In (001) foils defect yields were much smaller because of the loss of glissile a/2<111> loops to the surface, but a<100> loops were still present in molecular ion irradiations. The habit planes of both a/2<111> and a<100> loops were consistent with nucleation on {110} planes by the Eyre-Bullough mechanism. These results are compared with recent molecular dynamics simulations of the effect of the mass of primary knock-on atoms on displacement cascades in iron.

Deleted: keV

Deleted: keV

Deleted: ½

Key words: radiation damage, displacement cascades, cascade collapse

1. Introduction

The mechanical properties of structural materials in nuclear reactors are degraded by microstructural changes caused by fast-neutron irradiation. A fast fission or fusion neutron can impart an energy of several tens of keV to a primary knock-on atom (PKA). The PKA then generates a branching series of collisions termed a displacement cascade. As a consequence several hundred vacancies and self-interstitial atoms (SIAs) may be created within a small highly disordered volume, typically of dimension ~10 nm. Most of the displacements caused by fast neutrons occur in cascades generated by PKAs with energy > 10 keV. Consequently displacement cascades have received a good deal of theoretical and experimental attention over many years. Despite this, some aspects of cascades are still poorly understood.

The main theoretical tool for investigating the primary damage state at the end of the displacement phase of the cascade (which occurs in a few picoseconds) has been molecular dynamics (MD). Simulations of cascades by the MD method have been aided in recent years by the development of better interatomic potentials and more powerful computers, allowing more realistic simulations of larger cascades (see e.g. [1-3]). Such simulations have demonstrated that clustering of both vacancies and SIAs can occur at short timescales within cascades. The longer-term evolution of cascades has been studied by Kinetic Monte-Carlo methods, and further clustering may occur (see e.g. [4,5]). Clustering within cascades may be studied experimentally by carrying out low-dose heavy-ion irradiations of thin-foils and analysing the resulting damage structures by transmission electron microscopy (see e.g. the reviews [6,7]). The heavy-ions mimic the PKAs produced by fast neutrons. In such studies it is usually the case that only the vacancy component of the damage is seen. In many materials resolvable vacancy loops are produced within individual cascades by a process of cascade collapse.

Particular attention in recent years has focussed on displacement cascades in α-Fe, primarily due to the likely use of low-activation ferritic steels in future fission and fusion reactors. Fe and ferritic alloys are unusual in that cascade collapse does not occur at low doses in cascades initiated by self-ions [8,9]. However it does occur in cascades initiated by more massive ions. The fraction of cascades which collapsed to form visible loops increases as the mass of the incident ion increases [8-10]. From this it has been inferred that the thermal-spike lifetime and the energy density and vacancy concentration in the cascade centre must play an important role in the formation of the vacancy clusters. Further, in contrast to other bcc metals, in α-Fe a mixed population of a/2<111> and a<100> perfect loops was observed.

The effect of the mass of the PKA on displacement cascade evolution in α-Fe has recently been modelled by Calder *et al.* using MD [3,11]. These authors simulated cascades of energy 5-30 keV with PKA masses chosen to represent C, Fe and Bi. Bi_2 and Bi_3 molecular ion irradiations were simulated by using two or three adjacent Bi atoms as PKAs, and giving each half or a third of the total energy and the same initial direction of motion. The PKA mass was found to have a large effect on the damage produced within

Deleted: PKOs

Deleted: -

Deleted: cascade collapse

Deleted:

Deleted: et al

Deleted: .

individual cascades. The higher the PKA mass, the higher the peak number of displaced atoms. Clustering of both vacancies and interstitials was observed, with the largest clusters in cascades produced by heavier PKAs. Clustering was particularly pronounced in molecular ion simulations. In 30 keV Bi_3^+ molecular ion cascades, nearly every event led to the production of a large vacancy loop and one or more interstitial loops. Most of the interstitial loops had Burgers vectors **b** = a/2<111>, although some loops produced by molecular-ions had **b** = a<100>. Vacancy loops generally had **b** = a<100>. The largest loops contained as many as 200 vacancies. The probability for the production of a<100> loops increased with the total cascade energy and was highest for Bi_3^+ simulations, lower for Bi_2^+, and lower again for Bi^+.

The results summarized in the paragraph above are in qualitative agreement with the early experimental work of Jenkins *et al.*. [9] in α-Fe mentioned above as well as more recent *in-situ* experiments in Fe and FeCr alloys [10]. However there have been no other systematic experimental studies in α-Fe of the effect of PKA mass, most likely because of the experimental difficulties of working in a ferromagnetic material with a strong tendency to oxidise. However the new MD simulations of Calder *et al.* [3, 11] have prompted us to resurrect some previously unpublished data in molybdenum, where we carried out irradiations using molecular ions in an attempt to explore systematically the effect of PKA mass and energy on cascade collapse. Mo, like α-Fe, is bcc but there is no difficulty in preparing high-quality foils. In Mo, the defect yield, defined as the fraction of cascades which collapse to give a visible loop, has been found to depend on the material purity, the irradiation temperature and the mass and energy of the ion [12-14]. Typically however the defect yields are considerably lower than in pure fcc metals irradiated under similar conditions, and so in this respect Mo somewhat resembles α-Fe.

Molecular ion irradiations provide a convenient method for exploring the effect of important cascade parameters [15-18]. Molecular ions will dissociate on impact, the atomic components producing cascades which overlap both spatially and temporally, so increasing both the average energy density and vacancy concentration in the region covered by the cascades compared with a single ion of the same total energy. In addition the thermal spike lifetime is likely to be longer since the cascade is more compact. The total disorder created by molecular implants has been shown to be greater than that created by the equivalent atomic implants in GaAs [15] and in Si and Ge [16-18]. Antimony ions were chosen for these experiments because of their suitable atomic mass and the fact that beams could be produced free from charge-exchange products [19].

The specific aims of the present experiments were as follows:

1. To examine the production of vacancy loops in atomic and molecular ion cascades in Mo, by measuring the fraction of ions which produced visible loops, and the dependence of the size distributions on the ion species, and thereby gain information on the role of different cascade parameters on cascade collapse.

2. To study the distribution of the Burgers vectors between the two possible perfect loop Burgers vector types, a/2<111> and a<100> in the molecular ion implants.

Deleted:
Deleted: Bi
Deleted: et al
Deleted: *et al*
Deleted: .
Deleted: -
Deleted: in the molecular ion implants
Deleted: .

3. To determine loop habit planes

2. Experimental Procedures

2.1 Specimen preparation

The starting material was Climet arc cast molybdenum rod supplied by the Climax Molybdenum Company. High purity single crystals were prepared by electron beam zone refining to produce seeded single crystals with two orientations, with normals close to either the [011] or the [001] pole. The zone refining and subsequent heat treatment procedures to reduce the carbon and gaseous impurities to a few ppm level have been described elsewhere [20]. The purity of the crystals was monitored by measuring their resistivity ratios. The measured values of $R_{293K}/R_{4.2K}$ were 6600 + 200 for the (011) crystal and 8800 + 300 for the (001) crystal.

Finally, the single crystal rods were cut into 3mm discs and then electro-polished to produce perforated specimens suitable for irradiation and electron microscopy.

2.2 Irradiation procedure

The thinned discs were irradiated at room temperature in a low-energy ion accelerator with beams of Sb^+, Sb_2^+ and Sb_3^+ions. Three total energies per ion were employed: 60, 120 and 180 keV. Most (011) foils received a dose of 10^{16} ions m^{-2}, while most (001) foils received a dose of 4 x 10^{15} ions m^{-2}. Some lower dose (10^{15} ions m^{-2}) molecular ion irradiations were also performed[2].

2.3 Electron Microscopy

After irradiation the foils were examined in a conventional electron microscope operated at 100kV. The foil was located in a double-tilt holder with the damage surface adjacent to the electron exit surface, and suitable areas were imaged under several different diffraction conditions. The conditions employed for each crystal orientation are summarised in table 1. The foil thickness was ~5ξ_g, where ξ_g is the two-beam extinction distance for a {011}-type reflection, equal to 23.2nm [21].

In the present work all measurements were made from micrographs of magnification 3 x 10^5 obtained under dynamical imaging conditions, i.e. with deviation parameter $s_g = 0$, where small defects located within 1.25 ξ_g of the surface exhibit a characteristic black-white contrast [22] (see also [23]). The defect densities were measured by comparing the same area imaged in several reflections and noting the total number of defects visible. The criterion for positive identification was that a defect should appear in at least two conditions. The defect sizes were measured using micrographs taken with $\mathbf{g} = 01\bar{1}$ and $s_g = 0$. Calculations by Saldin *et al.* [24] suggest

[2] At these doses little cascade overlap occurs, so that we are looking essentially at individual cascade events. The doses correspond approximately to 0.001-0.01 dpa.

Deleted: , and so gain information on the mechanism of loop production.¶

Formatted: Numbered + Level: 1 + Numbering Style: 1, 2, 3, … + Start at: 1 + Alignment: Left + Aligned at: 18 pt + Tab after: 36 pt + Indent at: 36 pt

Formatted: Indent: Left: 36 pt

Deleted: .

Deleted: 6580

Deleted: 8750

Deleted: keV

Deleted: keV

Deleted:

Deleted: Table

Deleted:

Deleted: and is

Deleted: .

Deleted: et

Deleted: a1

that for these imaging conditions the ratio of image size to true defect size is approximately unity.

The directions of Burgers vector **b** and loop normal **n** of the small loops were analysed by comparing the symmetry of the observed dynamical images with the theoretically calculated images from known loops. The details of this approach have been discussed by Häussermann, Rűhle and Wilkens [25], Eyre Maher and Perrin [26,27] and Holmes, Eyre, English and Perrin [28] and are summarized in [23]. English, Eyre and Holmes [29] discussed in detail the method of analysing the geometry of a mixed population of edge and non-edge perfect loops in bcc metals, and this forms the basis of the analysis employed here. Essentially, the experimental images obtained under the standard imaging conditions are compared with the images computed for the possible loop geometries at these imaging conditions. By image matching it is possible to determine both the Burgers vector and to estimate the loop normal in a wide variety of cases.

Particularly useful images are those formed when **g.b** > 1 or **g.b** = 0. Some examples are illustrated in figure 1, which are image simulations made using the program described in ref. [30] for the case of a **b** = a/2[$\bar{1}1\bar{1}$] loop in a foil with normal **z** = [011] and imaged in **g** = $21\bar{1}$, $01\bar{1}$ and $2\bar{1}1$. Five loop normals are illustrated, lying between **n** = [$01\bar{1}$], which corresponds to a likely nucleation plane according to the Eyre-Bullough mechanism [31], and the edge configuration with **n** = [$\bar{1}1\bar{1}$]. It can be seen that the **g.b** = 1 and **g.b** = 2 images retain the same basic form for all loop normals although the angle of the black-white interface rotates with **n**, while for **g.b** = 0 the symmetrical 'butterfly' image obtained for the pure edge loop is progressively distorted as **n** approaches [$01\bar{1}$]. The characteristic interface structure of the **g.b** = 2 images is particularly valuable for defect analysis. A full description of the form of the images from non-edge loops can be found in [27], see also [29] and pp 46-49 in reference [23].

Deleted: , and

Deleted: Figure

Deleted: ,

3. Results

Figure 2 illustrates the damage microstructures in (011) foils produced by irradiation with Sb^+ and Sb_3^+ ions at total ion energies of 60 and 180 keV. In all cases small black-white images of dislocation loops are visible. Qualitatively it can be seen that the loop number density increased either as the number of atoms in the ion increased at constant ion energy, or as the total ion energy increased at constant ion mass.

Deleted:

Deleted: keV

Figure 3 shows similar irradiations of (001) foils. For Sb^+ implants, no damage was observed at an ion energy of 60 keV, while increasing the ion energy to 180 keV resulted only in a very low loop density. For molecular Sb_3^+ ions, loops were observed after all the implantations, with an increase in loop density and sizes when the ion energy was increased from 60 to 180 keV. For each irradiation condition illustrated it is clear that the loop density in the (001) foils is significantly lower than in the (011) foils. This is only partly due to the lower dose (see section 3.1 below).

The majority of the loop images in both figures 2 and 3 are consistent with layer 1 vacancy loops. The loop depths and consequently their nature were confirmed by stereo microscopy for selected irradiations. For the 120 and 180 keV Sb^+ implants of (011) foils, some layer 2 vacancy loops were present. In molecular ion irradiations at low doses (10^{15} ions m^{-2}) where cascades are well separated, we looked for evidence for multiple loops arising from wide separation of the atoms in the molecular ion. No such evidence was found.

We now present quantitative results, which are most conveniently described in terms of the defect yields, the loop geometries and the image size distributions.

3.1 Defect yields

Tables 2a and 2b show the measured defect yields for the (011) and (001) foils respectively. Consider first the (011) foils. Each row in table 2a gives the yields at a constant energy per ion. It can be seen that the yields increased on going from Sb^+ to Sb_2^+ to Sb_3^+; typically the yield tripled on going from Sb^+ to Sb_3^+. Each column in table 2a shows the effect of increasing the ion energy at constant ion mass. In each case the yield increased on going from 60 to 120 keV by a factor of two or more. A further increase in ion energy to 180 keV resulted in a smaller increase in yield, and indeed the yield appeared to saturate at ~0.3 for Sb_3^+ ions. At a constant energy per atom (i.e. 60 keV Sb^+. 120 keV Sb_2^+, 180 keV Sb_3^+) shown on the diagonal of table 2a, the yields increased in the ratio 1 : 3.5 : 7, whereas the number of atomic 60 keV cascades increased only in the ratio 1:2:3. This result highlights the important influence of overlapping cascades produced by the molecular ions.

In the (001) foils (table 2b), the low density of defects in the Sb^+ and Sb_2^+ irradiations meant that there was considerable error in estimating the defect density. However, the Sb_3^+ results show that the yield was approximately proportional to the ion energy.

It has been found in this study (see section 3.2 below) and in other studies of bcc metals [32, 10] that suitably orientated perfect loops produced close to the specimen surface may glide out of the foil. This would lead to a decrease in the measured yield, which would be dependent on the local foil orientation and loop morphology. No correction has been made for this effect in tables 2a and 2b, while an estimate of its probable magnitude is made in section 4.3.1.

3.2 Loop geometry analysis

3.2.1 (011) foils

For all irradiation conditions the Burgers vectors of a large majority of loops at this foil orientation were distributed between the two a/2<111> variants with **b** in the plane of the foil, that is, **b** = a/2 $[11\bar{1}]$ and **b** = a/2 $[\bar{1}1\bar{1}]$. At **z** = [011] these Burgers vectors give **g.b** = 0 images in **g** = $2\bar{1}1$ or $21\bar{1}$ respectively. It was possible to analyse the geometries

Deleted: Figures
Deleted: Layer
Deleted: Layer
Deleted: ,
Deleted: Table
Deleted: Table
Deleted: Table
Deleted: ,
Deleted: Table
Deleted: Table
Deleted: Consistent with earlier work, for
Deleted:

of 65-70% of the visible loops by noting if and how such images were distorted from the symmetric "butterfly" generated by edge loops. In this way non-edge loops could be identified and their habit planes estimated, and a determination made on which {110} plane they had likely nucleated (see figure 1 and references [29] and [23]). The results of an analysis of this sort for the case of a foil irradiated with 120 keV Sb_2^+ ions is shown in table 3, which gives detailed results of Burgers vector determinations and probable loop nucleation planes for three areas (a-c) of the same foil. The great majority of loops exhibited distorted **g.b** = 0 images typical of non-edge loops, with fewer than 3% showing the symmetrical 'butterfly' of pure edge loops. There was no significant variation in either Burgers vector or loop normal distributions between the three areas. Loops were evenly distributed between the two variants, and 60-70% had loop normals lying between $[01\bar{1}]$ and the direction of the Burgers vector, implying an edge-on $(01\bar{1})$ nucleation plane. Note that at this orientation it was not possible to distinguish between loops with **b** = a/2$[11\bar{1}]$ which had originated on the $(10\bar{1})$ or the (110) plane, or between loops with **b** = a/2$[\bar{1}1\bar{1}]$ which had originated on the $(10\bar{1})$ or the $(\bar{1}10)$ plane.

The general pattern seen in table 3 was found in most other cases at this foil orientation, with the exception of foils irradiated with 120 and 180 keV Sb_3^+ ions to a dose of 10^{16} ions m^{-2}. In these cases the loop densities were high, such that the loop-loop separation was of the order of the loop diameter, and it was observed that there were local inhomogeneities in the distributions of Burgers vectors and loop normals. Figure 4 shows three neighbouring areas (a, b and c) of the same foil in a specimen which had been irradiated with 10^{16} 180 keV Sb_3^+ ions m^{-2} and imaged in **g** = $2\bar{1}1$. It can be seen that the number of |**g.b**| = 2 images increases from fgure 4(a)-(c), indicating a change in the ratio of loops with **b** = a/2$[11\bar{1}]$ and **b** = a/2$[\bar{1}1\bar{1}]$. The detailed analysis is given in table 4, and confirms that the ratio of edge-on Burgers vectors was indeed different in each area. The distribution of loop normals was approximately the same in areas a and b, but in area c far fewer loops seemed to have nucleated on the edge-on $(01\bar{1})$ plane and most had nucleated on either $(1\bar{1}0)$ or (101). The defect yield in area c was also lower than areas a and b. This complex behaviour should be compared with the results at a lower loop density presented in table 3 for 120 keV Sb_2^+ ions, where little variation in **b** or **n** was found.

In foils implanted with molecular ions some loops were found that could not be analysed as having a/2<111> Burgers vectors. This is illustrated in figure 5, which shows an area of a foil irradiated with 180 keV Sb_3^+ ions and imaged in dynamical dark-field conditions in the three diffraction vectors g = 200, $2\bar{1}1$ and $2\bar{1}\bar{1}$. The arrowed loops show black-white contrast with interface structure typical of |**g.b**| > 1 in all three images. This pattern can only arise from loops with a[100] Burgers vectors [27],where |**g.b**| = 2 for all three reflections. Table 5 shows the fraction of a[100] loops for different irradiation conditions. It can be seen that some a[100] loop formation occurred with all the molecular ions. The fraction of a[100] loops increased with ion energy, and at a given energy was higher for irradiations with Sb_3^+ ions than for Sb_2^+ ions. No evidence was found for loops with inclined a[010] or a[001] Burgers vectors.

Deleted: Figure
Deleted: Table
Deleted: Table
Deleted: /m2
Formatted: Not Superscript/ Subscript
Formatted: Superscript
Deleted: where
Deleted: qualitatively
Deleted: Figure
Deleted: Table
Deleted: T
Deleted: Figure

Detailed inspection of the a[100] loops arrowed in figure 5 and of similar images taken in different diffraction conditions revealed that the black-white interfaces were not all parallel, indicative of different loop normals **n**. From the degree of rotation of the black-white interface of images from the pure edge configuration it was possible to determine the approximate direction of **n** [29]. More than 50% of the loops had **n** within ~15 degrees of the edge configuration. Many of the others had **n** close to <011>. In all conditions where a[100] loops were present, their images were consistent with nucleation on an {011} plane, followed by rotation on the glide cylinder partially or completely towards the pure edge configuration.

3.2.2 (001) foils

It was only in foils irradiated with Sb_3^+ ions that the loop densities were high enough for a detailed analysis of the loop geometries to be made. The analysis is illustrated in figure 6, which shows a specimen irradiated with 120 keV Sb_3^+ ions and imaged in diffraction vectors **g** = 200 (figure 6a) and **g** = 020 (figure 6b). A large majority of loops fall into one of two categories. The loops labelled A show typical $|\mathbf{g}.\mathbf{b}| > 1$ type contrast in **g** = 200 while in **g** = 020 they exhibit characteristic $|\mathbf{g}.\mathbf{b}| = 0$ images. The loops labelled B show the reverse contrast, with $|\mathbf{g}.\mathbf{b}| = 0$ images in **g** = 200 and $|\mathbf{g}.\mathbf{b}| > 1$ images in g = 020. This suggests the assignment of **b** = a[100] to loops A and **b** = a[010] to loops B. This assignment was confirmed by comparison with computed images of loops with these Burgers vectors [29]. This conclusion that most loops in (001) foils irradiated with Sb_3^+ ions have a<100> Burgers vectors was also found at other ion energies. In the 120 keV Sb_3^+ irradiation illustrated in figure 6 fewer than 2% of the loops had **b** = a/2<111>. For 180 keV Sb_3^+ irradiations the fraction of a/2<111> loops was <5%. In the case of the loops produced by 60 keV Sb_3^+ ions, 30% of the loops were too small for analysis, but the remainder were analysed as having a<100> Burgers vectors. Thus the defect yields given in table 2b for (001) foils in fact demonstrate how the production of edge-on a<100> loops is determined by ion energy and mass. Within experimental error the Burgers vectors were equally distributed between a[100] and a[010]. No evidence of a[001] Burgers vectors was found in (001) foils imaged at **z** = [011], where computations show that loops with this Burgers vector would produce strong images.

Deleted: Figure

Deleted: 001

Deleted: Figure

Deleted: Figure

Deleted: Figure

Deleted: Figure

Formatted: Font: Bold

Deleted: Table

Again loop normals were determined by comparing the experimental images with computed images of loops with loop normals between <110> and the Burgers vector [29]. The distribution of loop normals was determined for the loops formed in the two higher-energy irradiations. The loop normals of the great majority of the loops were consistent with nucleation on the edge-on (110) and $(1\,\bar{1}\,0)$ planes and then rotation towards the edge configuration. For one foil irradiated with 120 keV Sb_3^+ ions, fewer than 8% of the loops had **n** within 10° of the edge configuration and more than 60% had **n** within 20° of the [110] or $[1\,\bar{1}\,0]$ directions.

3.3 Image size distributions

Mean image diameters are given in table 6, while selected image size distributions are presented in figure 7. In the case of (011) foils, an increase in the ion energy at constant ion mass resulted in a shift in the peak in the distribution to larger sizes and an increase in the maximum loop size, causing an increase in the mean image size (see columns in table 6). This trend was most pronounced for irradiations with Sb_3^+ ions and is illustrated in figure 7a-c. The same trends were seen on increasing the ion mass at constant ion energy (see the rows in table 6), and are illustrated for the most pronounced case of 180 keV ions in figure 7d-f. In (001) foils, it was only possible to obtain distributions for irradiations with Sb_3^+ions. Here, the mean image diameter (last column of table 6) increased with ion energy. There were no significant differences between the size distributions in (001) foils (figure 7g-i) and (011) foils irradiated with the same ions (figure 7a-c). For 60 keV Sb_3^+ ions, the larger mean image diameter in the (011) foils was caused by a greater fraction of loops with diameters > 4.0 nm. Finally, a detailed analysis of the loops formed after the 180 keV Sb_3^+ irradiations revealed that there were no significant differences between the size distributions in (011) foils of the a<001> loops and the a/2<111> loops, although no a[001] loops were identified with image diameters less than 2.5 nm. This last observation may simply be due to the low number densities with consequent bad statistics.

Deleted: Table
Deleted: Figure
Deleted: 8
Deleted: Table
Deleted: Figure
Deleted: 8a
Deleted: Table
Deleted: Figure
Deleted: 8d
Deleted: Table
Deleted: Figure
Deleted: 8g
Deleted: Figure
Deleted: 8a
Deleted: -

4. Discussion

4.1 Consistency of observations with the Eyre-Bullough mechanism for loop formation in bcc metals

Deleted: .

In bcc metals it has long been considered that loops may form by the Eyre-Bullough mechanism [31]. This mechanism envisages that point-defects aggregate initially on {110} planes to form faulted a/2<111> loops. The very high stacking fault energy of molybdenum causes such loops to unfault , most probably when the loop diameter is still < 1nm, and so below the resolution limit(~ 2nm) for TEM. The mechanism is described in a typical case by the shear reaction:

Deleted: regarded
Deleted: <1nm,
Formatted: Font: (Default) Times New Roman
Deleted:

$$a/2[01\bar{1}] + a/2[100] \rightarrow a/2[11\bar{1}]$$

In section 3.2.1 it was demonstrated that a significant number of non-edge a/2<111> loops were observed, and that it was possible to determine on which {110} plane they had likely nucleated, i.e. the data in the present paper are consistent with the mechanism in the case of a/2<111> vacancy loops.

Deleted: provide further evidence for

In addition found that that our observations of the loop habit planes of a<100> vacancy loops in Mo are also consistent with this mechanism (see section 4.3). As in the case of a/2<111> loops, the normals found for a<l00> loops suggested nucleation on {110} planes. The shear is described by the reaction of the type:

Deleted: we have a new result that
Deleted: probably produced by

$$a/2[011] + a/2[0\bar{1}1] \rightarrow a[001]$$

There is also evidence in the literature for the Eyre-Bullough mechanism, at least in the production of vacancy loops. For example, Häussermann [12] observed a/2<110> faulted loops in ion-irradiated tungsten, and many a/2<111> loops had large shear components, consistent with habit planes close to {110}. Several other studies have found a/2<111> loops in ion-irradiated bcc metals with normals close to <110> directions, or with normals lying between <110> and the direction of the Burgers vector, e.g. [12, 29]. However, we have also to note that in recent MD simulations of the configurations of self-interstitial clusters in Fe, Tapesa *et al* [33] found that the habit plane of a/2<111> loops corresponding to the minimum energy configuration at 0K tends towards the {110} plane. Thus, the observation of <110> loop normals can only be said to be consistent with the Eyre-Bullough mechanism, not proof of its occurrence. However, we note that the effect of surface image forces on the resultant loop configurations is also consistent with the Eyre-Bullough mechanism. For example, Jäger and Wilkens [34] have shown in heavy-ion irradiation experiments in tungsten that their results may be explained if the Eyre-Bullough mechanism is operative, and the unfaulting reaction is influenced by the close proximity of the surface, which is within 10 nm of the damage region. Unfaulting reactions which result in loops with Burgers vectors pointing towards the surface tend to be favoured.

The Eyre-Bullough mechanism has not yet been identified explicitly in MD simulations of vacancy loops e.g. [1-3]. Indeed Marian *et al.* [32] claim that it does not occur for a<100> interstitial loops, and proposed an alternative mechanism whereby such loops could be produced. In contrast, Tapesa et al [33] found in their MD study of α-Fe evidence for transformation of faulted a/2<110> interstitial loops to a<100> loops at 0K. However, dynamical simulations suggested that small a/2<111> interstitial loops are more stable than other loops despite the lower energy of a/2<110> loops at 0K.

There could be several reasons why the mechanism has not been seen for vacancy loops in MD simulations. First, it is intrinsically difficult to interpret MD data in terms of mechanisms. In particular, vacancy loops form in the highly-disordered cascade core as the thermal spike cools, and the morphology of such loops at an early stage in their evolution is difficult to discern in the MD visualizations. Second, the simulations may not have been run for long enough for the mechanism to be recognised. For example, in recent simulations by Calder *et al.* (see [11] and section 4.4 of this paper) vacancy clusters first appeared quite late in the displacement phase, typically after >10-15 ps, whereas interstitial clusters appeared after 1-2 ps. Recognisable vacancy loops did not form before 20s, while the simulations were terminated at ~30 ps. Third, it might simply be the case that the Eyre-Bullough mechanism does not occur in these simulations.

4.2 Formation of a<100> loops in molecular ion irradiations

We have found that in (001) foils, a larger fraction of the loops had Burgers vectors a<l00> in Sb_3^+ irradiations compared with Sb_2^+ irradiations at the same energy. Further, at constant ion mass the number density of a<100> loops increased with ion energy for both foil orientations. At first sight the observation of a<100> loops in molybdenum is

Deleted: strong
Deleted: found strong evidence fo
Deleted: r
Formatted: Font: Italic
Deleted: ¶
Deleted: ¶
Deleted: , either for
Deleted: or interstitial
Deleted: o
Deleted: et al
Deleted: 2
Deleted: However, there
Deleted:
Deleted: *al*
Deleted: The strong experimental evidence for the Eyre-Bullough mechanism in vacancy loop formation suggests that its occurrence or absence in MD simulations may be a good indicator of how realistic are the simulations. We recommend that modelers should look for this mechanism explicitly.
Deleted: .

unexpected, because such loops are expected to have much larger energies than a/2<111> loops. Little *et al.* [35] have calculated for several bcc metals the probability that an a/2<110> interstitial loop unfaults to a loop with Burgers vector a<100> rather than to a/2<111>. They employed-a simple continuum model to represent the propagation of the unfaulting partial dislocation across the faulted loop, and then used the relative magnitude of the energy barriers to give the relative probabilities. For molybdenum at room temperature, the probability of a<100> loop formation is extremely low (1 in 10^{19}). It is likely that the unfaulting probabilities for vacancy loops are similar.

Molecular ion cascades will occur closer to the surface than single ion cascades of the same energy. However, it is not likely that the occurrence of a<100> loops is due to the influence of the surface. Elastic interactions with the surface will reduce the energies of both a/2<111> and a<100> loop types, but by only a small amount in comparison with the large energy difference between the two geometries (see the discussion in Section 4 of Jenkins *et a1.* [9]).

A more likely explanation for the increased probability for the formation of a<100> loops is the increased average energy density and thermal spike lifetimes in the centre of molecular ion cascades. The calculated probability of a<100> loop formation only approaches the observed frequency if a temperature close to the melting point is achieved in the cascade region (when the calculated probability of 10^{-4} compares with the observed probability of 10^{-3} -10^{-4}). Within cascades with a high density of deposited energy, the effective temperature of the region may be considerably higher than the host lattice temperature, leading to a "thermal spike". Sigmund [36] calculated that the cumulative average energy density (expressed as a temperature) decreased with increasing ion energy, but that the lifetime of the thermal spike increased. A value for the cumulative average energy density (eV/atom) for atomic ion cascades can be arrived at from this work. For molecular ion cascades, a value can be obtained by assuming that the average energy density in a cascade created by an Sb_m^+ ion with total energy mE is m times that of an atomic Sb^+ ion with energy E. For Sb_3^+ ions with energy between 60 and 180 keV, the estimated energy density is always of the order of the sublimation energy (6.8 eV/atom) for molybdenum, supporting the supposition that high temperature regions occur within Sb_3^+cascades.

It is therefore possible to account for a<100> loop formation by postulating that there are high temperature regions within some of the molecular ion cascades, which persist during the initial formation and growth of the faulted loop. Within such regions the probability of unfaulting to a<100> is significant. The increased lifetime of these zones at higher ion energies allows a greater number of faulted loops to nucleate, grow and unfault.

An interesting comparison can be made between the a<l00> loop formation in molybdenum and that previously observed in α-Fe [8,9]. In contrast to the present results in (011) foils, where even in the most favourable case <2% of the loops had Burgers vectors a<l00>, in (011) foils of α-Fe about 50% of the loops were identified as a<l00> after 80 keV W^+ ion irradiation [9]. It is interesting to note that the calculations

Deleted: et al
Deleted: 33
Deleted:
Formatted: Font: Italic
Deleted: 34
Deleted: keV

presented in ref. [35] show that the probability of a/2<110> loops unfaulting to a<100> loops is considerably higher in α-Fe than in molybdenum, in agreement with the observed trends. a<100> loops appear to be more stable in α-Fe than in other bcc metals. Very recent calculations by Dudarev *et al.* [37] have explained the greater relative stability of a<100> loops in α-Fe at high temperatures in terms of an elastic instability, driven by spin fluctuations.

Deleted: 3

Deleted: et al

Deleted: 35

4.3 Insight into vacancy loop formation in (011) foils

4.3.1 *Estimates of true defect yields*

We first consider briefly the possible effect on the defect yield of the loss of loops by glide to the surface. In (011) foils, the perfect loops formed after unfaulting from the edge-on $(01\bar{1})$ plane have **b** = a/2$[11\bar{1}]$ or a/2$[\bar{1}1\bar{1}]$). Since these Burgers vectors lie in the foil plane, none of these loops will be lost to the surface. This is not true for other {110} nucleation planes, where a proportion of loops have a component of **b** towards the surface and will be lost. An estimate of the true defect yield can be obtained by identifying and counting those non-edge loops which had originated on the edge-on $(01\bar{1})$ plane (i.e. loops with a loop normal **n** lying between $[01\bar{1}]$ and the edge-on Burgers vectors (a/2$[11\bar{1}]$or a/2$[\bar{1}1\bar{1}]$). These figures are shown in tables 3 and 4. Typically about 60-70% of loops were found to have originated on the $(01\bar{1})$ plane. About 60-70% of the observed yield therefore derives from loops which nucleated on $(01\bar{1})$. If we further assume that nucleation on any of the six {110} planes is equally likely, the true yield is six times this fraction of the observed yield, i.e. the true yield is about four times the observed yield. Such a correction would imply that for 120 and 180 keV Sb_3^+ molecular ion irradiations the true yield is close to unity.

Deleted: Tables

In table 7 we present the corrected defect yields, cascade efficiencies, and vacancy retention efficiencies. The cascade efficiency is defined as the fraction of vacancies surviving in each cascade to form a loop, whilst the vacancy retention efficiency is defined as the percentage of calculated displacements which are retained in loop form. It differs from the cascade efficiency by including those cascades which do not form visible loops. The number of displacements in the cascade has been calculated using the internationally accepted formalism due to Norgett, Torrens and Robinson [38].

Deleted: Table

The assumption in the argument above that loop nucleation on any of the six {110} planes may not be correct. At higher doses the inhomogeneous distributions of **b** and **n** (table 4) suggest that loop nucleation is probably influenced by the strain fields of existing nearby loops. It is possible therefore that we have underestimated loop losses to the surface in the estimates above. This would not however affect the conclusion that the true yields under high-energy molecular ion irradiation are close to unity.

Deleted: Table

Deleted: In addition, Jäger and Wilkens [36] have shown in heavy-ion irradiation experiments in tungsten that the unfaulting reaction may be influenced by the close proximity of the surface which is within 10nm of the damage region. Unfaulting reactions which result in loops with Burgers vectors pointing towards the surface tend to be favoured.

4.3.2 Vacancy loop formation in atomic ion cascades

The calculated number of displacements in atomic-ion cascades is proportional to the ion energy. However the mean size of loops is only weakly dependent on the ion

energy (table 6). The number of vacancies in a loop of mean area increases by only 30% on going from 60 keV Sb^+ ions to 180 keV Sb^+ ions. This leads to a decrease in the cascade efficiency with increasing ion energy, which drops by a factor of about two on going from 60 keV to 120 keV, with a further small decrease at 180 keV (table 7). However, the increase in the corrected defect yield with ion energy leads to the interesting result that the fraction of calculated displacements which are retained in loop form is approximately independent of ion energy at ~7%-10%. As the ion energy increases, cascades will become larger and the average vacancy concentration within the cascade volume will decrease. In the cascade region large fluctuations in the vacancy concentration will occur, leading to sub-cascade formation. It is within these regions of local high vacancy concentration that vacancy loops are likely to nucleate.

The combination of increasing defect yield and decreasing cascade efficiency with increasing ion energy implies that the probability of vacancy aggregation in a region of the cascade is greater in high energy implants, but that a smaller proportion of the vacancies created are able to participate in loop growth. Thus we conclude that in high energy cascades, only those vacancies in the immediate vicinity of the growing vacancy cluster are able to diffuse to it.

4.3.3 Vacancy loop formation in molecular ion cascades

As a first estimate, we have assumed in calculating cascade efficiencies that the number of displacements produced in a Sb_m^+ (m = 2 or 3) molecular ion cascade of energy mE is the sum of the displacements produced in m single-ion cascades of energy E. The likelihood of thermal spike effects mean that this is likely to be only an approximate estimate.

Our results show that the production of vacancy clusters is strongly enhanced in cascades created by diatomic and triatomic ions. In particular:

- For 120 keV and 180 keV Sb_3^+ ions, the corrected defect yields are close to unity. As no evidence was found of multiple loops in low dose molecular ion irradiations, this implies that the formation of a vacancy loop occurs in nearly all cascades. These yields are considerably higher than those obtained with atomic implants. Such high yields are common in fcc metals but have only been found previously in bcc metals irradiated with very heavy ions, e.g. [9].

- The vacancy retention efficiency is strongly enhanced by increasing the ion mass at constant ion energy. The data in table 7 show that a factor of 5-8 more vacancies are retained in loop form for Sb_3^+ ions than for Sb^+ ions of the same energy.

- At constant energy per atom in the molecular ion, the ratio of defect yields for Sb^+, Sb_2^+ , and Sb_3^+ ions increases more sharply (by 1:4:7) than the ratio of total ion energies (1:2:3).

Deleted: Table

Deleted: Table

Deleted:

Deleted: The

Deleted: likelihood of thermal spike effects means that this is likely to be an underestimate

Deleted: .

Deleted: .

Deleted: .

Deleted: Table

These trends in the data demonstrate that vacancy loop formation in cascades produced by molecular ions is strongly favoured. It is tempting to associate this with the increased energy density in molecular ion cascades. This is because molecular ions are expected to dissociate on impact, the different components creating overlapping displacement cascades. If spatial overlap were complete in the collisional phase of the cascade, then single and molecular ions of the same energy ***per atom*** might be expected to produce cascades of similar volumes. However, Jenkins and English [39] have studied the disordered zone sizes produced in ordered Cu_3Au by Sb^+ atomic and molecular ions. In such experiments the disordered zones give a measure of the size and shape of the region where many replacements have occurred. The data obtained in these experiments suggested that disordered zone sizes are determined more by the ***total*** ion energy than by the energy per atom. For example, disordered zones created by 150 keV Sb_3^+ ions were very similar in size to those created by 150 keV Sb^+ ions, but had mean diameters about 30% larger than those produced by 100 keV Sb_2^+ ions and ~60% larger than those produced by 50 keV Sb^+ ions. The shapes of disordered zones produced by 150 keV Sb_3^+ ions were however more regular than those produced by 150 keV Sb^+ single ions. These findings may be evidence that cascade overlap is incomplete. It is nevertheless likely that there are regions of overlap within molecular ion cascades where particularly high energy densities do occur, and these may lead to dynamic events which trigger loop formation. Insight into such processes is now available from MD simulations. This is described in the next section.

Deleted: of high total energy density

Deleted: would

Deleted: 37

4.4 Comparison with MD simulations

There have been no MD simulations of molecular ion cascades in Mo, but recently such simulations have been made in "α-Fe" by Calder *et al.* [3,11]. In these studies, the PKA mass was also varied in single-ion cascades. Strongly enhanced vacancy clustering was found in cascades initiated by heavy PKAs, and was particularly pronounced in molecular ion cascades, with the formation of dislocation loops. Calder *et al.* followed the atomic exchanges leading to the production of Frenkel pairs. The paths from surviving SIAs to their originating vacancies were followed. Such paths were usually very tortuous. When all such paths were displayed simultaneously, tangled, so-called spaghetti-regions were defined, within which most displacements had occurred. Calder *et al.* did not find a strong variation in the total volume of these spaghetti-regions for different ions of the same energy, but the *shape*s of these regions were more spherical for cascades produced by molecular ions than those produced by single-ions of the same energy. Such spaghetti regions should correlate with the disordered zones formed within cascades in ordered alloys, and so these finding are consistent with our results on molecular-ion irradiated Cu_3Au mentioned above [39]. Qualitatively one might expect the thermal spike lifetime to be longer in a spherical cascade because of its smaller boundary area compared with cascades of more complex shape, so that energy is transferred to the surrounding matrix more slowly. In addition the local regions of high deposited energy density and vacancy concentration would likely be more proximate in spherical cascades than in cascades of more irregular shape. These effects may enhance vacancy clustering. The conclusion that conditions of long thermal spike lifetimes, and

Deleted: et al

Deleted: et al

Deleted: et al

Deleted: 37

high local energy densities and vacancy concentrations favour collapse has also been drawn in previous MD simulations [40-42] and experiments [6, 9].

The actual process of point-defect clustering in the MD simulations seems not to have been completely elucidated. In Calder *et al*'s simulations, interstitial clusters, including loops with **b** = a/2<100> and a<100>, formed at the peripheries of the cascade regions within 1-2 ps of the initiation of the cascade by some sort of dynamic process, which seemed to involve the production of a shock wave which propagated out from the cascade core immediately after the displacement phase of the cascade. Interstitial loop formation did not seem to involve conventional nucleation and growth processes, but was reminiscent of loop punching. The formation of large interstitial clusters was a good predictor of strong vacancy clustering at the cascade core later in the evolution of the cascade. Indeed vacancy loop production was always found in association with interstitial clustering. In an earlier MD study of cascades in Fe produced by 50 keV self-ions, Soneda *et al.* [42] found a single example of vacancy loop production (out of 100 cascades simulated), and in this case too large interstitial clusters formed at the periphery of a high energy-density region early in the cascade evolution. Vacancy loops formed in the thermal spike phase of the cascade after about 20-30 ps, by a process of collapse of the vacancy-rich core in a process similar to the classical picture. These loops all had Burgers vectors a<100>. Although a<100> loops are in reality a particular feature of Fe, the potential used in these simulations of "α-Fe" would not have been expected to favour the formation of a<100>loops over a/2<111> loops. Nevertheless the simulations do predict vacancy loop formation and its dependence on ion mass in good accord with our experiments.

The most marked difference between recent MD simulations and experiments is that in experiments interstitial loops are not seen at low doses. In thin-foil experiments such as those described here, this may be due partially to preferential loss of SIAs and small interstitial clusters to the surfaces. Loss of interstitials to the surface and consequent enhanced vacancy clustering due to reduced recombination have been found in MD simulations of cascade damage in Fe by Stoller [43]. The fraction of vacancies contained in clusters increased as the cascade initiation site approached the surface. A similar result was found by Gao and Bacon for near-surface displacement cascades in Ni_3Al [44]. Experimental evidence that the surface influences cascade collapse has been presented by Műller *et al.* [45]. In Ni_3Al, the defect yield in cascades created by 50 keV Ta^+ ions at 573K decreased from about 0.7 for cascades centred close to the ion-entry surface to about 0.2 for cascades centred at a depth of more than 10 nm. There was a similar trend but smaller decrease in yield in Cu_3Au irradiated at room temperature with 50 keV Ni^+ ions. It does therefore seem to be the case that the strong vacancy clustering seen in our experiments may be partly attributed to thin-foil irradiations.

Loss of SIAs and interstitial loops to the surface does not however give a complete explanation of the difference between MD simulations and experiments. In Calder *et al.*'s MD simulations [11] many of the interstitial loops were of a size that would be resolvable in the electron microscope. In an (011) foil some interstitial loops would be expected to have their glide cylinders in the plane of the foil and such loops

Deleted: 38
Deleted: -40
Formatted: Font: Italic
Deleted: et al
Deleted: 40
Deleted: 41
Deleted: 42
Deleted: et al
Deleted: 43
Deleted: et al

would not be lost to the surface. However none was found. In earlier thin-foil experiments in ion-irradiated Cu, Stathopoulos [46] analysed the nature of ~ 500 loops of sizes 1-5 nm. by careful measurements of their depths, and found no interstitial loops. Moreover, cascade collapse to vacancy loops with relatively high probability but with few if any small interstitial loops has been found in several low-dose neutron experiments in bulk materials. For example, Muncie *et al.* [47] found in low-dose (3 x 10^{21} neutrons m^{-2}) irradiations of Cu at 80°C that loops of sizes< 4nm were predominantly of vacancy nature, and were present at a number density consistent with the expected concentration of energetic cascades and defect yields found in heavy-ion experiments. Some larger interstitial loops were observed but at concentrations much less than vacancy loops. In similar experiments in dilute Cu-Ge alloys, Shepherd *et al.* [48] found that the number of interstitial loops depended on the alloy composition, suggesting that they had formed by nucleation and growth involving long-range diffusion rather than a cascade process. In low-dose neutron irradiations of Cu_3Au, loops were always associated with disordered zones, and were found at cascade cores, again suggested their nature was vacancy [49]. It seems therefore that there is little experimental evidence for the formation directly in cascades of interstitial loops large enough to be resolved in the electron microscope.

Deleted: 44

Deleted: (e.g.,

Deleted: et al

Deleted: 45

Deleted: et al

Deleted: 46

Deleted: concentration

Deleted: 47

Deleted: ¶

5. Summary and Conclusions

1. Cascade collapse in Mo has been studied by employing molecular ion irradiations. Collapse was strongly enhanced in molecular ion cascades compared with single ion cascades of the same total energy, with increases both in defect yields and in loop sizes. These findings are in qualitative agreement with recent MD simulations of cascades in α-Fe which also found enhanced clustering in molecular ion cascades.

2. In (011) foils most loops had Burgers vectors **b** = a/2<111> lying in the plane of the foil. However in molecular ion irradiations a small fraction of loops with **b** = a[100] was also found. This fraction was higher for Sb_3^+ than for Sb_2^+ ions and also increased with ion energy. a<100> loops were also produced in molecular ion irradiations of (001) foils.

3. Vacancy loops of both a/2<111> and a<100> types may have formed by the Eyre-Bullough mechanism, which involves initial nucleation of a faulted loop on a {110} plane.

4. The experiments described here suggest that the thermal spike lifetime, cascade energy density and vacancy concentration are important factors in cascade collapse.

Deleted: .

Deleted: L

Deleted: are believed to

Deleted: Thermal spike effects may be responsible for unfaulting to the energetically less favourable a<100> loops.

Deleted: ¶
¶

Acknowledgements

We acknowledge with thanks discussions with Dr A F Calder, including discussions of unpublished MD simulations. We thank Dr Zhongfu Zhou for assistance in the preparation of figure 1.

References

1. A. F. Calder and D. J. Bacon, J. Nucl. Mater. **207** 25 (2000).
2. Yu. N. Osetsky, D. J. Bacon, B. N. Singh, B. Wirth, J. Nucl. Mater. **307-311** 852 (2002).
3. A. F. Calder, D. J. Bacon, A. V. Barashev and Yu. N. Osetsky, Phil. Mag. Lett. **88** 43 (2008).
4. N. Soneda and T. Diaz de la Rubia, Phil. Mag. **A78** 995 (1998).
5. T.S. Hudson, S. L. Dudarev, M-J Caturla and A. P. Sutton, Phil. Mag. **85** 661 (2005).
6. C. A. English and M. L. Jenkins, Mat. Sci. Forum **15-18** 1003 (1987).
7. M. L. Jenkins, M. A. Kirk and W. J. Phythian, J.Nucl. Mater. **205** 16 (1993).
8. C. A. English, M. L. Jenkins and B. L. Eyre , Nature **263** 400 (1976).
9. M. L. Jenkins, C. A. English and B. L. Eyre, Phil. Mag. **38** 97 (1978).
10. Z. Yao, M. Hernández-Mayoral, M. L. Jenkins and M. A. Kirk, Phil Mag **88** 2851 (2008)
11. A. F. Calder, D. J. Bacon, A. V. Barashev *et.al.* , Phil. Mag.(2009) this issue.
12. F. Häussermann, Phil. Mag. **25**, 561 and 583 (1972).
13. C. A. English, B. L. Eyre, A. F.Bartlett and H. N. G. Wadley, Phil.Mag. **35** 533 (1977).
14. M. L. Jenkins, M. A. Kirk and W. J. Phythian, J.Nucl. Mat. **205** 16 (1993).
15. J.A. Moore, G. Carter and A.W.Tinsley Rad.Effects, **25**, (1975).
16. G. Foti, G. Vitali, and J.A. Davies, Rad. Effects **32** 187 (1977).
17. J.A. Davies, G.Foti, *et al.*, Phys. Rev. Lett. **34** 14441 (1975).
18. D. A. Walker and R. S. Thompson., Rad. Effects **32** 135 (1977).
19. D.G.Beanland, J.H. Freeman, and C.A.English in "Application of Ion Beams to Materials" (Eds G.Carter, J.S.Culligon, and W.A. Grant, IOP (1976)) p262.

Deleted: ,
Deleted: ,
Deleted: ,
Deleted: 1978
Formatted: Font: Bold
Deleted: ,
Deleted: ,
Deleted: ,
Deleted: L
Deleted: ,
Deleted: ,
Formatted: Font: Bold
Deleted: ,
Deleted:
Deleted: &
Deleted: ,
Formatted: Font: Bold
Deleted: ,
Deleted: Radiation
Formatted: Font: Bold
Deleted: ,
Deleted: 1975,
Deleted: 49-51.
Deleted: G.
Deleted: J.A.
Deleted: et al
Deleted: ,
Deleted: ,
Deleted: ,
Deleted:
Deleted: ,

20. D.J.Capp, H.W.Evans, and B.L.Eyre, J. of Less Common Metals, **40** 9 (1975).

21. A. Howie, and Z.S. Basinski, Phil. Mag. **17** 1039 (1968).

22. M. Rűhle Phys. Stat. Sol. **19** 263 (1967).

23. M. L. Jenkins and M. A. Kirk, Characterisation of Radiation Damage by Transmission Electron Microscopy, (Taylor and Francis), ISBN 0 7503 0748 X (hbk) (2001).

24. D. K. Saldin, A.Y. Stathopoulos and M.J. Whelan, Proc. Roy. Soc. **292** 523 (1979).

25. F. Häussermann, M. Rűhle and M. Wilkens, Phys. Stat. Sol. b, **50** 445 (1972).

26. B. L. Eyre, D. M. Maher and R. C. Perrin, J. Phys. F: Met. Phys. **7** 1359 (1977).

27. B. L. Eyre, D. M. Maher and R. C. Perrin, J. Phys. F: Met. Phys**. 7** 1370 (1977).

28. S. M. Holmes, B. L. Eyre, C. A. English and R. C. Perrin, J. Phys. F: Met. Phys. **9** 2307 (1979)

29. C. A. English, B. L. Eyre and S.M. Holmes J. Phys. F: Met. Phys**. 10** 1065 (1980).

30. Z. Zhou, M. L. Jenkins, S. L. Dudarev, A. P. Sutton and M. A. Kirk, Phil. Mag. **86** 4851 (2006)

31. B.L. Eyre and R. Bullough, Phil. Mag. **12** 31 (1965).

32. J. Marian, B. D. Wirth and J. M. Perlado, Phys. Rev. Lett. **88** 255507 (2002)

33. K. Tapesa, A. V. Barashev, D. J. Bacon and Yu. N. Osetsky, J. Nucl. Mat. **361** 52 (2007)

34. W. Jäger and M.Wilkens, Phys. Stat. Sol. a, **32** 89 (1975).

35. E.A.Little, R. Bullough, and M. Wood, Proc. Roy. Soc. A, **373**, 565 (1989).

36. P. Sigmund Appl. Phys. Lett. **25(3)** 169 (1974).

37. S. L. Dudarev, R. Bullough and P. M.Derlet, Phys. Rev. Lett. **100** 135503 (2008).

38. M. J. Norgett, M. T. Robinson and I.M. Torrens, Nucl. Eng. Des. **33**, 48 (1975).

39. M.L. Jenkins and C.A. English., J. Nucl. Mat. **108** and **109** 46 (1982)

40. V. G. Kapinos, Yu. N. Osetsky and P. A. Platinov, J. Nucl.Mater. **170** 60 (1990).

Deleted: ,
Deleted: ,
Deleted:
Deleted: ,
Formatted: Font: Bold
Deleted: ,
Deleted: ,
Deleted: ,
Deleted: ,
Deleted: ,
Formatted: Left
Deleted: L
Deleted: ,
Deleted: 12,
Formatted: Font: Bold
Deleted: *Marion*
Formatted: Font: Italic
Formatted: Font: Bold
Deleted: ,
Formatted: English (U.S.)
Formatted: List Paragraph, Left, No bullets or numbering, Widow/Orphan control
Formatted: Font: Bold
Formatted: English (U.S.)
Formatted: No bullets or numbering
Deleted: ics
Deleted: ers
Deleted: ,
Formatted: Dutch (Belgium)
Formatted: List Paragraph, Left, No bullets or numbering, Widow/Orphan control
Deleted: ¶
¶
W. Jäger and M.Wilkens, Phys. Stat. Sol. a, **32**, 89 (1975).¶
Formatted: Indent: Left: 18 pt
Deleted: &
Deleted: ,
Deleted: ,

41. V. G. Kapinos, Yu. N. Osetsky and P. A. Platinov, J. Nucl. Mater. **173** 229 (1990).

42. N. Soneda, S. Ishino and T. Diaz de la Rubia, Phil. Mag. Lett. **81** 649 (2001).

43. R. E. Stoller, J. Nucl. Mater. **307-311** 935 (2002).

44. F. Gao and D. J. Bacon, Phil. Mag. **A75** 1603 (1997).

45. S, Műller, M. L. Jenkins *et al.*, Phil. Mag. **A75** 1625 (1997).

46. A. Y. Stathopoulos, Phil. Mag. **A44** 355 (1981).

47. J. M Muncie, B. L. Eyre and C.A.English, Phil. Mag. **A52** 309 (1985).

48. B. W. O. Shepherd, M. L. Jenkins and C. A. English, Phil. Mag. **A56** 485 (1987).

49. C. A. English and M. L.Jenkins, J. Nucl.Mater. **96** 341 (1981).

Deleted: ,
Formatted: Font: Bold
Deleted: ,
Formatted: Font: Bold
Formatted: Font: Bold
Deleted: ,
Deleted: and
Deleted: ,
Deleted: et al
Formatted: Font: Bold
Deleted: ,
Formatted: Font: Bold
Deleted: ,
Formatted: Font: Bold
Deleted: ,
Deleted: ,
Deleted: L
Deleted: ials
Deleted: ,

Tables

Table 1 Imaging Conditions Employed

Foil orientation	Diffraction vector **g**	Foil normal
155 023 $\bar{1}35$ 135	$\pm 01\bar{1}$ ± 200 $\pm 2\bar{1}1$ $\pm 21\bar{1}$	Close to [011]
$\{\bar{1}17\}$ {117} {015} {105}	± 110 $\pm 1\bar{1}0$ ± 200 ± 020	Close to [001]

Table 2a Defect Yields for (011) foils

Ion keV	Sb^+	Sb_2^+	Sb_3^+
60	0.04 ± 0.01	0.08 ± 0.01	0.12 ± 0.015
120	0.07 ± 0.015	0.14 ± 0.01	0.32 ± 0.02
180	0.10 ± 0.01	0.17 ± 0.01	0.28 ± 0.01

Table 2b Defect Yields for (001) foils

Ion keV	Sb^+	Sb_2^+	Sb_3^+
60	-	~0.0003	0.02 ± 0.005
120	-	~0.003	0.04 ± 0.01
180	~0.002	~0.006	0.07 ± 0.01

Table 3 Loop normal distributions in an (011) foil irradiated with 120 keV Sb_2^+ ions.

Area	Nucleation plane			Ratio
	$[01\bar{1}]$	Inclined [110] or $[10\bar{1}]$	Inclined $[1\bar{1}0]$ or [101]	$a/2[11\bar{1}]/a/2[\bar{1}1\bar{1}]$
a	70%	20%	10%	1.23
b	72%	12%	16%	0.91
c	63%	21%	16%	0.96

Table 4 Loop normal distributions and defect yields in an (011) foil irradiated with 10^{16} 120 keV Sb_3^+ ions m^{-2}, for the three areas shown in figure 4.

Deleted: Figure

Area	Nucleation plane			Ratio a/2[11$\bar{1}$]/a/2[$\bar{1}$1$\bar{1}$]	Defect Yield
	[01$\bar{1}$]	Inclined [110] or [10$\bar{1}$]	Inclined [1$\bar{1}$0] or [101]		
a	65%	34%	1%	5.35	0.25 ± 0.03
b	55%	38%	7%	1.8	0.30 ± 0.03
c	27%	12%	61%	0.3	0.18 ± 0.02

Table 5 Fraction of loops with **b** = a[100] in (011) foils.

Ion keV	Sb^+	Sb_2^+	Sb_3^+
60	0	<0.1%	0.3%
120	0	<0.1%	0.7%
180	0	0.2 – 0.4%	1.7%

Table 6 Mean Image Sizes (nm)
(Error in mean is ± 0.1 nm)

Foil Normal	[011]			[001]
Ion keV	Sb^+	Sb_2^+	Sb_3^+	Sb_3^+
60	3.2	3.6	4.0	3.6
120	3.3	4.7	5.0	5.0
180	3.6	4.8	5.7	5.8

Table 7 Corrected defect yields, cascade efficiencies and vacancy retention efficiencies for (011) foils

	Corrected Defect Yield			Cascade Efficiency[#]			Vacancy retention efficiency		
Ion keV	Sb^+	Sb_2^+	Sb_3^+	Sb^+	Sb_2^+	Sb_3^+	Sb^+	Sb_2^+	Sb_3^+
60	0.15	0.29	0.35	0.43	0.53	0.83	0.06	0.15	0.29
120	0.30	0.55	1.05	0.24	0.49	0.55	0.07	0.27	0.58
180	0.49	0.82	1.09	0.21	0.36	0.50	0.10	0.30	0.55

[#] In calculating the cascade efficiency it has been assumed that molecular ions create the same number of displacements as the appropriate number of atomic ions.

Figure captions

Figure 1: Simulated black-white contrast images of edge and non-edge perfect loops in Mo. The simulations are for a first-layer loop with **b** = a/2[$\bar{1}\,1\,\bar{1}$] loop in a foil with normal **z** = [011] and imaged in **g** = $2\,1\,\bar{1}$, $0\,1\,\bar{1}$ and $2\,\bar{1}\,1$. Five loop normals **n** are illustrated lying in the (011) plane between **n** = [$0\,1\,\bar{1}$] and **n** = [$\bar{1}\,1\,\bar{1}$]. Foil thickness 5.25, loop depth 5.10, loop radius 0.1, in units of the extinction distance ξ_{110}.

Figure 2: Damage microstructures in (011) foils produced by irradiation with Sb^+ and Sb_3^+ ions at total ion energies of 60 keV and 180 keV. In each case the diffraction vector **g** = $0\,1\,\bar{1}$.

Figure 3: Damage microstructures in (001) foils produced by irradiation with Sb^+ and Sb_3^+ ions at total ion energies of 60 keV and 180 keV. In each case the diffraction vector **g** = 200.

Figure 4: Three areas (a, b and c) of the same foil in a specimen which had been irradiated with 10^{16} 180 keV Sb_3^+ ions m^{-2} and imaged in **g** = $2\,1\,\bar{1}$. The Burgers vectors and loop normal distributions are not uniform, see the text for details.

Figure 5: An (011) foil irradiated with 180 keV Sb_3^+ ions and imaged in dynamical dark-field conditions in the three diffraction vectors **g** = 200, $2\,1\,\bar{1}$ and $2\,\bar{1}\,1$. The arrowed loops have Burgers vector a[100].

Figure 6: An (001) foil irradiated with 120 keV Sb_3^+ ions and imaged in diffraction vectors (a) **g** = 200) and (b) **g** = 020. Loops have either a[100] or a[010] Burgers vectors, see text for details.

Figure 7: Image size distributions:
Top row: (011) foils irradiated with Sb_3^+ ions of different energies;
Middle row: (011) foils irradiated with single and molecular180 keV ions;
Bottom row: (001) foils irradiated with Sb_3^+ions of different energy.

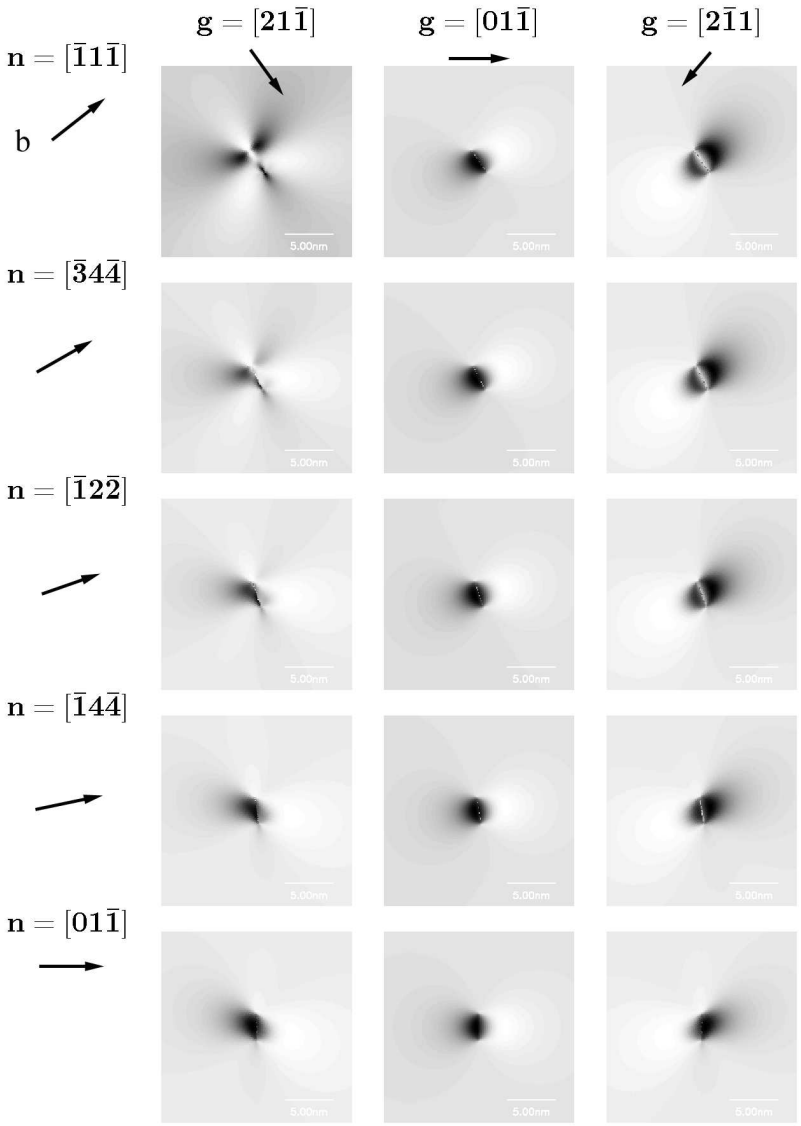

Figure 1
114x159mm (300 x 300 DPI)

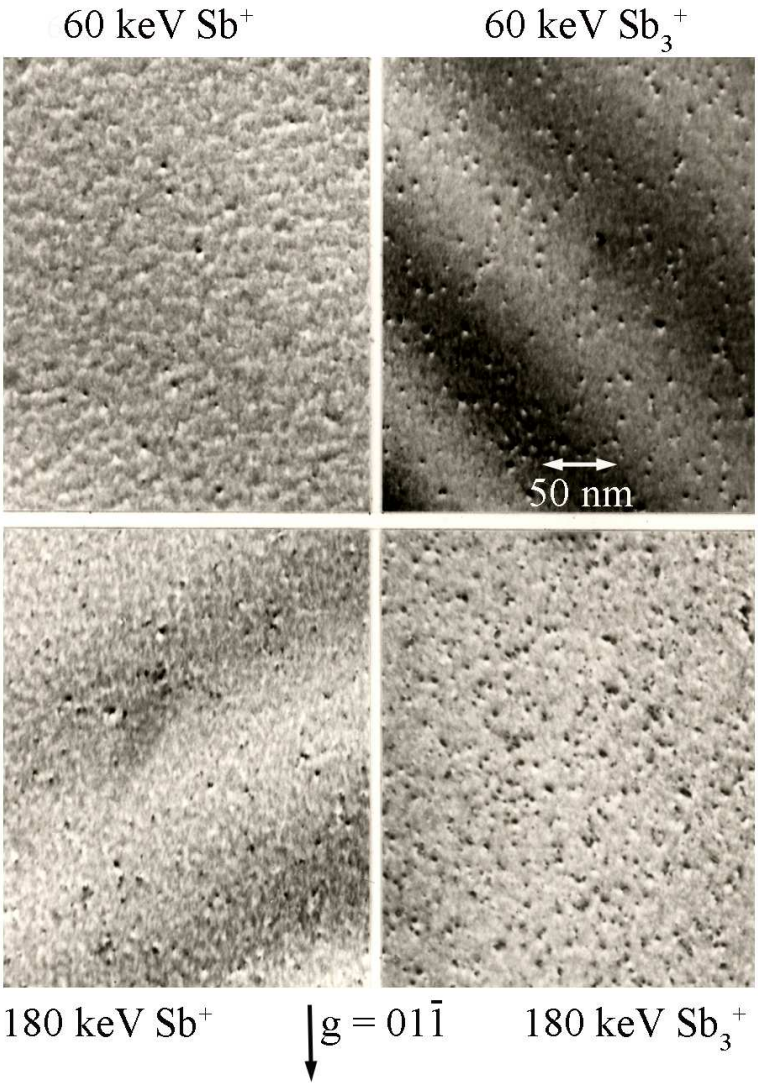

Figure 2

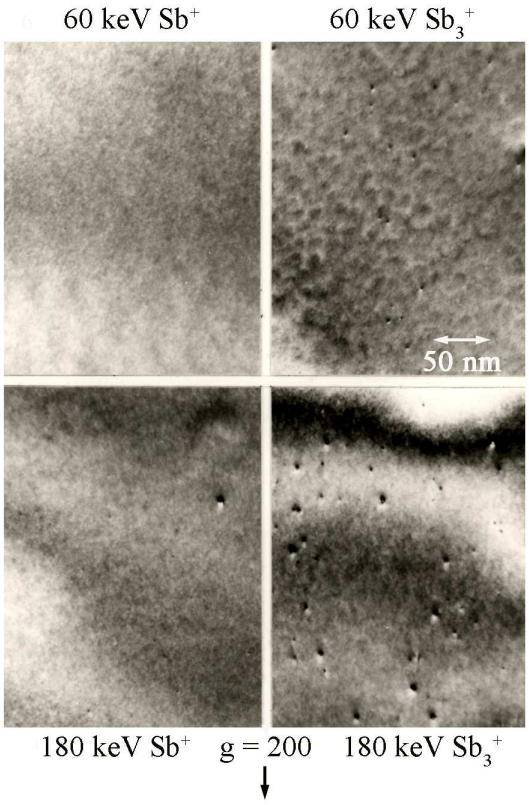

Figure 3

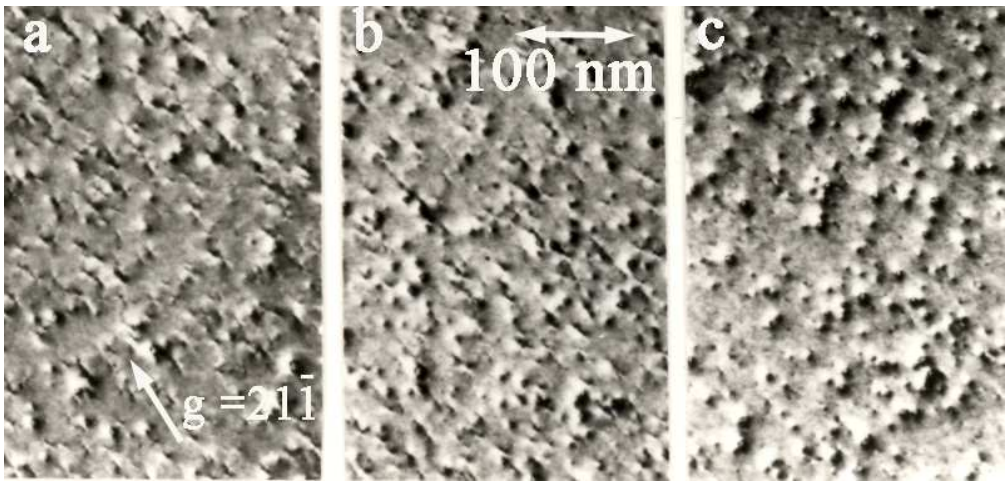

Figure 4
135x64mm (150 x 150 DPI)

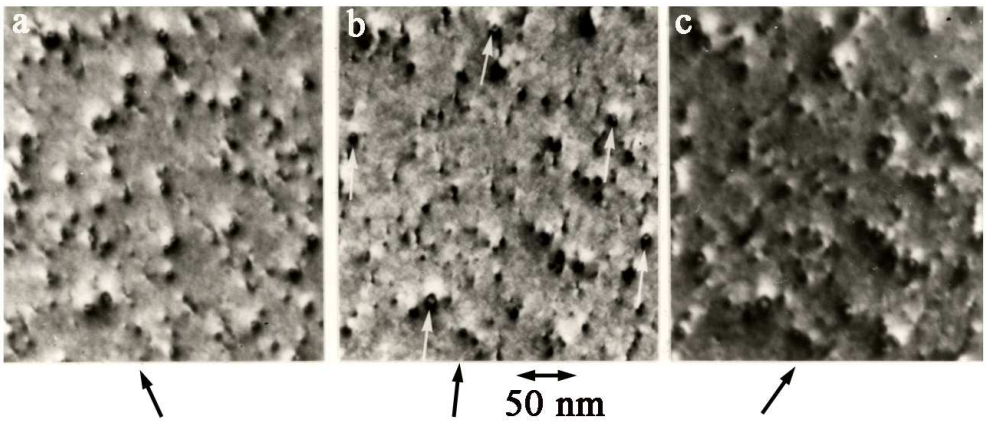

Figure 5

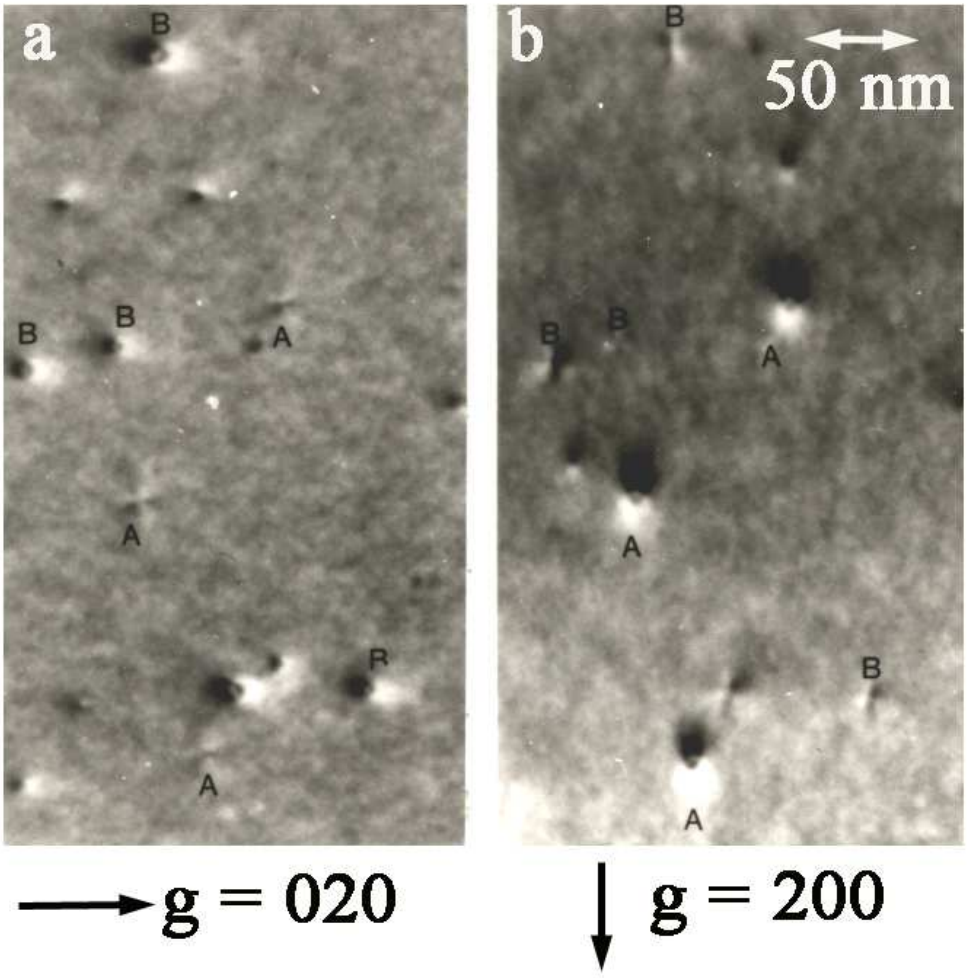

Figure 6

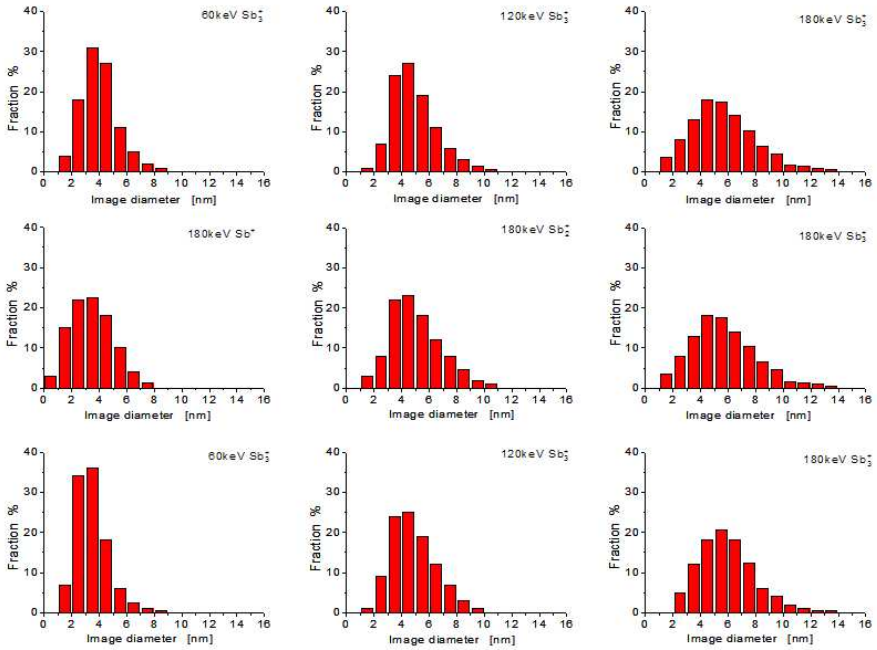

Figure 7
318x233mm (72 x 72 DPI)